8th Japan-China-Korea Workshop on Microgravity Sciences
For Asian Microgravity Pre-Symposium

Interferometric Observation of Temperature Distributions in the Smoke Experiment

Yuki KIMURA[*], Katsuo TSUKAMOTO

Abstract

Interferometric observation was attempted to the gas evaporation method to investigate the homogeneous nucleation and growth process of nanoparticles in vapor phase. For the first step, temperature distribution around evaporation source was measured with respect to the source temperature in the gas evaporation method for the first time in a half century. We visualized a condensation of smoke particles in gas phase and temperature history including a cooling rate of produced particles after nucleation was recognized. Homogeneously condensed WO_3 nuclei initially maintain their temperature for ~5 ms and then cool down with a rate of ~5×10^4 K/s. The degree of supersaturation during the nucleation was at least as high as 10^7.

1. Introduction

Homogeneous nucleation is rarely seen in natural environment on the Earth. In contrast, homogeneous nucleation is very important process in a formation of cosmic dust particles in universe. Smoke experiments [1-3] may be a suitable experimental method for reproduction of cosmic dust particles, because nanoparticles form via vapor phase condensation similar with the dust formation in gas ejecta of evolved stars. In universe, although 99% atoms exist as a gas phase, there are 1% solid particles, which will become building blocks of planetary systems and life. Initially, cosmic dust particles must be condensed via homogeneous nucleation at least first one. Using the gas evaporation method, fine particles with the size of several nm to ~1 μm are directly produced from the gas phase and recognized nanoparticles have a crystalline habit similar with the bulk crystal even in such tiny particles [4].

When an evaporant is initiated in an inert gas, the evaporated vapor subsequently cools and condenses in the gas atmosphere, i.e., solid grains are obtained via homogeneous nucleation from the vapor phase. Therefore it can be assumed that nucleation occurs far from the equilibrium state, but it is not obvious how far condensation takes place. Although there are some reports concerning homogeneous and heterogeneous nucleation from solution phases [5], there have been few reports concerning homogeneous nucleation from a vapor phase in recent years [6,7]. To know the formation process of nanoparticles in smoke, temperature distribution around evaporation source was measured using thermocouple and found that nanoparticles grow by coalescence even at the temperature is lower than the melting point [8]. In contrast, there is no report concerning nucleation and limited study in view of crystal growth for smoke experiment, although significant numbers of smoke experiments have been performed so far.

To understand the formation process of cosmic dust particles, some experimental studies were performed concerning nucleation process [9-13]. However, quantitative discussion based on data obtained by non-contact method has not been achieved so far. Here, we report a first direct visualization during a condensation of smoke particles in a vapor phase using interferometric technique, which has often employed for solution crystal growth [14-16], and determine the temperature gradients around an evaporation source and temperature history of produced particles in the gas evaporation methods by contact-free method.

2. Experimental Procedure

2.1 Smoke chamber

A smoke chamber, which has a Mach-Zehnder type interferometer, was newly constructed based on a new concept to observe the temperature and concentration distributions in a smoke. The work chamber used was a stainless-steel cylinder 16 cm in inner diameter and 24 cm in height with two view ports of ICF152 for optical observation and eight ports of ICF70 for electrodes, temperature measurements and so forth and connected to a high-vacuum exhaust of a turbo molecular pump (210 L/s) through a valve at its bottom. An evaporation source was set in the chamber at the center of the larger view ports. After evacuating the chamber down to ~10^{-4} Pa, the valve was

Department of Earth and Planetary Materials Science, Graduate School of Science, Tohoku University, Sendai 980-8578, Japan
(E-mail: ykimura@m.tohoku.ac.jp)

closed and then Ar (99.9999 % in purity) and/or oxygen (99.999 % in purity) gases were introduced into the chamber at 1.0×10^4 Pa. The pressure was monitored by a capacitance manometer (ULVAC CCMT-1000D) and a pirani/cold cathode combination gauge (Preiffer PKR 251). Smoke particles are produced in the gas atmosphere due to electrical heating of the evaporation source. Source temperature was measured using a pyrometer ($\lambda= 0.8 - 1.6$ μm, FTZ2, Japan Sensor Co.). The source temperatures were also measured occasionally using Pt-PtRh 13% and chromel-alumel thermocouples with 0.1 mm in diameter for corrective the measurement value of the pyrometer. Total gas pressures and temperatures were recorded using a data logger with an interval of 200 ms.

2.2 Optics

A Mach-Zehnder type interferometer with a polarized He-Ne laser at 632.8 nm (50 mW) was prepared on an Al board with 30 mm in thick in a clean booth (class 20). The Al board moves gently up and down with 1 mm/s to observe various position of the smoke. **Figure 1** shows a top view of the optical path. An evaporation source was prepared as long as possible (45-70 mm in length) certainly parallel to the optical path to make higher column density, which is an advantage to detect the tiny change of the refractive index, because refractive index of typical gas pressure (Ar: 1.0×10^4 Pa) to produce nanoparticles by the gas evaporation method is very small (($n-1)_{Ar}$ =

$2.599 \times 10^{-5} \pm 0.008 \times 10^{-5}$ for 632.8 nm at 293.15 K [17]). Using this experimental setup, we can detect a difference of refractive index smaller than 1×10^{-6}, which is corresponding to a difference between the refractive indexes of Ar gas 1×10^4 Pa at 298 K and at 302 K. Interferogram was observed using a HD-TV camera (SONY HDC-X300) and recorded by a HD recorder (Panasonic AG-HPG20). Radiation from the evaporation source was cut by an IR filter (>50% at 330-680 nm).

3. Temperature distributions

Tungsten wire (99.95% in purity) with 0.3 mmϕ and 70.0 mm in length was prepared as an evaporation source as an initial simplest case. When the tungsten wire is electrically heated in a pure Ar gas atmosphere of 1.0×10^4 Pa, ambient Ar gas is warmed up and the optical path length is changed depend on the temperature. The chamber is large enough to avoid making a distortion by elevation of source temperature. Here, we assumed that optical path length is changed only the 70 mm in length around the evaporation source. The validity was confirmed from the small difference (much less than 50 K) between source temperature measured by a pyrometer and a
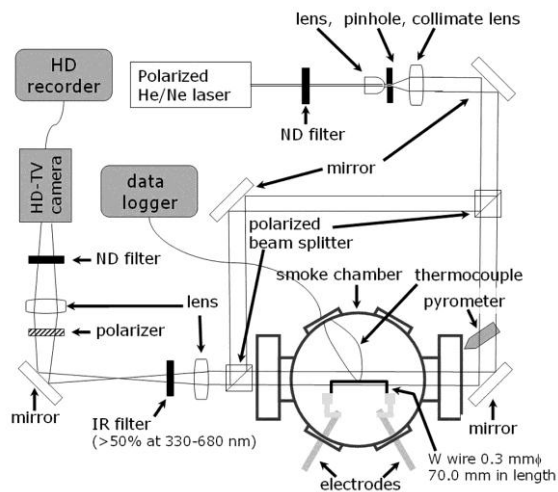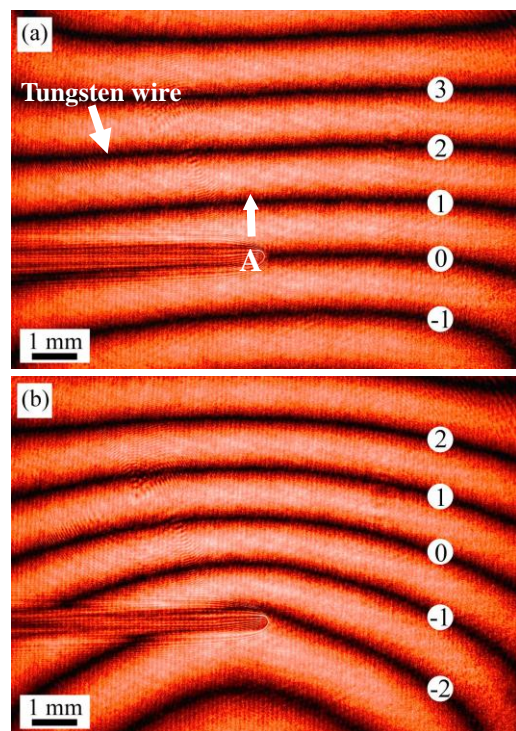

Fig. 1 Optical set up of a Mach-Zehnder type interferometer. Tungsten (W) wire, which was prepared in the smoke generator, is an evaporation source certainly parallel to the optical path. Polarized He/Ne laser with 50 mW at 632.8 nm were used. Source temperature was measured using a pyrometer and occasionally thermocouple and recorded using a data logger. IR filter is to cut the radiation from the evaporation source. Interferogram was captured using a HD-TV camera and recorded by a HD recorder.

Fig. 2 Typical interferograms of steady states around the evaporation source of tungsten wire at (a) room temperature and (b) 1200°C in Ar gas of 1.0×10^4 Pa, . The numbers with the fringes in each figure have been corresponded, i.e., guide for the shift. View direction of these interferograms that is from left to right of the chamber, and the shape of tungsten wire will be known in Fig. 1. The tungsten wire has a 70 mm in depth at A.
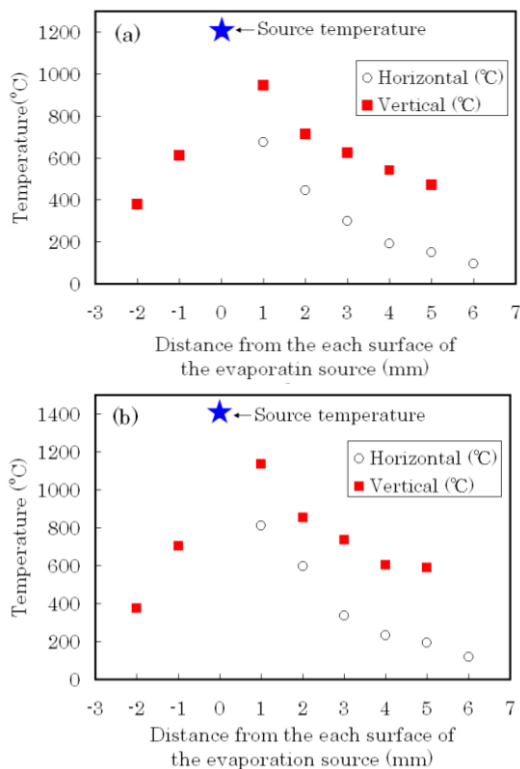
Fig. 3 Temperature gradients around the evaporation source heated at (a) 1200°C and (b) 1400°C, respectively, in Ar gas of 1.0×10^4 Pa. Stars show source temperatures measured by a pyrometer. Open circles show temperatures at the position from the evaporation source to the horizontal direction. Filled squares show temperatures at the position from bottom to upper at the center of evaporation source.

thermocouple, and the temperature just above the evaporation source determined from interferogram[18]. Temperature dependence of refractive index of Ar $N_{Ar}(T,P)$ at temperature T (^{o}C) and pressure P (Torr) was expressed by $N_{Ar}(T,P) - 1 = (N(0,760) - 1) / (1 + \alpha * T) * P / 760$, where α is coefficient of volume expansion. Because partial pressure of metallic tungsten is negligible during the heating due to extremely low vapor pressure (10^{-5} Pa at 2235°C), difference of the optical path length is only a result of thermal heating. As the result, we can obtain the temperature profile around the evaporation source. **Figure 2** shows typical interferograms at the source temperature of (a) 24°C and (b) 1200°C, respectively. The fringes have been labeled to recognize the movement of the fringes. The fringe "0" has been shifted in two lines by heating.

Figure 3 shows the temperature gradients around evaporation source at the source temperature (a) 1200°C and (b) 1400°C, respectively. The temperature gradients 1 mm from the evaporation source at 1200°C are ~520 K/mm for horizontal, ~580 K/mm for lower and ~250 K/mm for upper the source,

respectively. In case of the source temperature at 1400°C, the temperature gradients for horizontal, lower and upper from the source are ~580 K/mm, ~690 K/mm and ~250 K/mm, respectively. Temperature elevation of the evaporation source generates thermal convection from bottom to top in **Fig. 2**. An egg like temperature profile is generated around an evaporation source due to blow of the cooler buffer gas against the source.

The velocity of the thermal convection was measured as functions of source temperature and pressure [19]. In case of present experimental condition, the velocity can be estimated as ~100 cm s^{-1}. Then cooling rates at the first 5 mm above the evaporation source can be roughly estimated ~1.4×10^5 K/s at 1200°C and 1.6×10^5 K/s at 1400°C, respectively.

4. Pressure distributions

When materials evaporate by thermal heating of the evaporation source and distribute concentrically from the source, degree of supersaturation at the below direction becomes largest at the same centric distance due to strong convection described in section 3. Since the rising vapor is accelerated and the down flow of the vapor is restrained due to the strong convection, partial pressure of evaporated vapor becomes highest at the below direction, i.e., degree of supersaturation below the source becomes highest in respect to a pressure distribution as well as the effect of temperature gradient. Therefore, it is concluded that homogeneous nucleation mainly occurs below the evaporation source.

WO$_3$ smoke shows up at the source temperature around 1300°C. **Figure 4** shows a typical interferogram of a WO$_3$ smoke. The WO$_3$ smoke was generated by a thermal heating of the source in a mixture gas of Ar 9.0×10^3 Pa and O$_2$ 1.0×10^3 Pa.
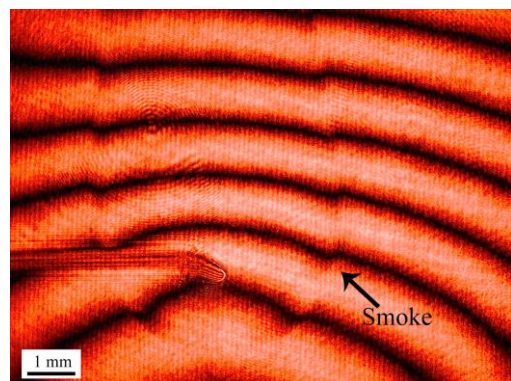

Fig. 4 A typical interferogram of steady state of a WO$_3$ smoke, which produced by a electrical heating of a tungsten wire in a mixture gas of Ar 9.0×10^3 Pa and O$_2$ 1.0×10^3 Pa. Significant change of the fringe to the lower direction shows existence of materials with higher refractive index than ambient environment, i.e., smoke of WO$_3$.

Since the difference of the refractive indexes of Ar and O_2 is very small, $\sim 10^{-7}$, temperature profiles can be applied to the smoke experiment with oxygen. The collected smoke particles were observed using a Hitachi H-8100 transmission electron microscope operated at an accelerating voltage of 200 kV at Tohoku University and were triclinic WO_3 nanoparticles with 20-200 nm in diameter.

Nucleation must be occurred at a highest supersaturation environment, where is ~ 1 mm below the evaporation source and the temperature is about at 600-700°C. Then, equilibrium vapor pressure "P_e" of WO_3 is $\sim 10^{-7}$ Pa. Since partial pressure "P" at the evaporation source at 1300°C is an order of 10^2 Pa, the degree of supersaturation "P/P_e" is 10^9 or somewhat lower due to vapor dilution by diffusion. When nuclei produced at the bottom site of the smoke, it follows the convection current and produces a smoke. The profile of the smoke from bottom to horizontal position overlaps a uniform temperature profile at 600-700°C. Namely, the temperature of the nuclei maintains 5 mm in flow distance after nucleation. Subsequently, grown nuclei cool down with a rate of $\sim 5\times10^4$ K/s. So far, it has been simply considered that the condensed nanoparticles in smoke immediately cool down with a rate of 10^4-10^5 K/s. However, our result implies a new view of a temperature history of a smoke particle with temperature maintain phase for 5 ms at the first stage soon after nucleation.

We are planning to do similar experiment under microgravity. Since the convection current will be suppressed, incubation time for nucleation and temperature history of smoke particles will be clearer. In addition, number density of the nuclei can be directly compared to the calculated values of a nucleation theory.

5. Conclusions

Temperature gradients of argon gas atmosphere around evaporation source were measured by non-contact method in-situ using interferometer. Since it is obvious that there is no heterogeneous nucleation cites around the evaporation source in the gas evaporation method, nanoparticles are condensed homogeneously from the vapor phase. Temperature gradients suggest nucleation occurs below the evaporation source and produced nanoparticles follow up a thermal convection. Then, the trajectory of the smoke overlaps a temperature profile. Accordingly, produced nuclei initially maintain their temperature for ~ 5 ms and then cool down with a rate of $\sim 5\times10^4$ K/s. The degree of supersaturation during the nucleation at 1300°C was at least as high as 10^7.

Acknowledgement

References

1) R. Uyeda: Morphology of crystals, Part B, ed. Sunagawa, 369, Terra, Tokyo, 1987).

2) K. Kimoto, Y. Kamiya, M. Nonoyama and R. Uyeda: Jpn. J. Appl. Phys., **2** (1963) 702.

3) J. A. Nuth, F.. J. M. Rietmeijer and H. G. M. Hill: Meteoritics & Planetary Science, **37** (2002) 1579.

4) R. Uyeda: Parity, **2** (1987) 4.

5) X. Y. Liu, K. Tsukamoto and M. Sorai, Langmuir, **16** (2000) 5499.

6) J. L. Schmitt, G. W. Adams and R. A. Zalabsky: J. Chem. Phys., **77** (1982) 2089.

7) G. W. Adams, J. L. Schmitt and R. A. Zalabsky: J. Chem. Phys., **81** (1984) 5074.

8) C. Kaito: Jpn. J. Appl. Phys., **17** (1978) 601.

9) J. A. Nuth and B. Donn: J. Chem. Phys., **77** (1982) 2639.

10) H. Kobatake, K Tsukamoto, H. Satoh: Journal of Crystal Growth, **279** (2005) 186.

11) Y. Kimura and J. A. Nuth III: The Astrophysical Journal Letters, **697** (2009) L10.

12) Y. Kimura, S. Sasaki, H. Suzuki, A. Kumamoto, M. Saito and C. Kaito: The Astrophysical Journal, **684** (2008) 1496.

13) Y. Kimura, J. A. Nuth III and F. T. Ferguson: Meteoritics & Planetary Science, **41** (2006) 673.

14) K. Tsukamoto, Faraday Discuss., **95** (1993) 183.

15) K. Onuma, K. Tsukamoto and S. Nakadate, Journal of Crystal Growth, **129** (1993) 706.

16) A. Srivastava, K. Tsukamoto, E. Yokoyama, K. Murayama and M. Fukuyama: Journal of Crystal Growth, **312** (2010) 2254.

17) Y. Clergent, C. Durou and M. Laurens: J. Chem. Eng. Data, **44** (1999) 197.

18) Y. Kimura, H. Miura, K. Tsukamoto, C. Li, T. Maiki: Journal of Crystal Growth, **316** (2011) 196.

19) S. Yatsuya, A. Yanagida, K. Yamauchi and K. Mihama: Journal of Crystal Growth, **70** (1984) 536.